Air-Intake Design Investigation for an Air-Breathing Electric Propulsion System

IEPC-2015-269／ISTS-2015-b-269

Presented at Joint Conference of 30th International Symposium on Space Technology and Science, 34th International Electric Propulsion Conference and 6th Nano-satellite Symposium
Hyogo-Kobe, Japan
July 4–10, 2015

Francesco Romano* , Tilman Binder† , Georg Herdrich‡ , Stefanos Fasoulas§
Institute of Space Systems (IRS), University of Stuttgart, Stuttgart, 70569, Germany

and
Tony Schönherr¶
The University of Tokyo, Bunkyo, Tokyo, 113-8656, Japan

An air-breathing electric propulsion system (RAM-EP) ingests the air of the residual atmosphere through an Air-Intake and uses it as propellant for an electric thruster. Key component of the system is the Air-Intake, which has the task of collecting atmosphere particles and directing them into the thruster, accompanied by compression. Studies have considered different configurations, and have shown the feasibility of the device. Within this paper an overview of the current Air-Intake designs is given. Results of DSMC simulations, performed with our in-house code PICLas, are presented and compared to those from the respective publications. Moreover, the influence of simplifying assumptions, such as free molecular or hyperthermal flow, is shown. Additionally, a simple analytical model based on transmittances and the balance of particle flows is derived, applicable for the analysis and further possible optimization of a generic Air-Intake design. The model is compared to the results of DSMC simulations and a sensitivity analysis of the basic parameters is performed. Regarding the assumption of hyperthermal flow, results shows that part of the particles will interact with the lateral structures of the Air-Intake and therefore will be scattered loosing their macroscopic velocity. Moreover, the implementation of straws into the Air-Intake simulations needed particular attention. A deeper investigation over their single transmittances has been done. Through the balancing model a sensitivity analysis over their L/R ratio has been performed and results show how a low ratio would lead to higher densities and collection efficiencies.

*Ph.D. Student, Institute of Space Systems (IRS), romano@irs.uni-stuttgart.de.
†Ph.D. Student, Institute of Space Systems (IRS), binder@irs.uni-stuttgart.de.
‡Head Plasma Wind Tunnels and Electric Propulsion, Institute of Space Systems (IRS), herdrich@irs.uni-stuttgart.de.
§Head Department of Space Transportation, Institute of Space Systems (IRS), fasoulas@irs.uni-stuttgart.de.
¶Assistant Professor, Dpt. of Aeronautics and Astronautics, schoenherr@al.t.u-tokyo.ac.jp.

Nomenclature

A_{in}	= Air-Intake Front Surface
A_{out}	= Air-Intake Outlet Surface
Ap	= Geomagnetic Index
BM	= Balancing Model
DSMC	= Direct Simulation Monte Carlo
ECR	= Electron Cyclotron Resonance
El.	= Element
F	= Thrust, Force
$F10.7$	= Solar Radio Flux at $\lambda = 10.7\,\text{cm}$
h	= Altitude
k_B	= Boltzmann Constant
L	= Length
m_p	= Particle Mass
$\dot{m}_{thr}$	= Mass Flow to Thruster
$n_{avg,ch}$	= Average Number Density in Chamber
n_{ch}	= Number Density in Chamber
n_{in}	= Number Density in Inflow
$n_{tot,in}$	= Total Number Density in Inflow
$\dot{N}_{accel}$	= Accelerated Particle Flow
$\dot{N}_{in}$	= Incoming Particle Flow
$\dot{N}_{thr}$	= Particle Flow to Thruster
$\dot{N}_{out}$	= Outlet Particle Flow
p_{ch}	= Chamber Pressure
p_{in}	= Inflow Pressure
R	= Radius
Rel. Dev.	= Relative Deviation
RAM EP	= Air-Breathing Electric Propulsion
S/C	= Spacecraft
T_{ch}	= Chamber Temperature
T_{in}	= Inflow Temperature
T_{wall}	= Wall Temperature
v_{ch}	= Velocity in Chamber
v_{in}	= Inflow Velocity
v_{out}	= Exhaust Velocity
v_z	= Velocity in z Direction
α	= Accommodation Coefficient
Γ	= Mass Flux (e.g. by Thermal Effusion)
η_c	= Collection Efficiency
$\Theta_{Clausing}$	= Backflow Transmittance following Clausing's Assumptions
Θ_{fast}	= Transmittance for Fast, Unscattered Particles
$\Theta_{intake1}$	= Transmittance for the Intake in Inflow direction
$\Theta_{intake2}$	= Transmittance for the Intake in Backflow direction
Θ_{out}	= Transmittance for the Outflow
$\Theta_{scattered}$	= Transmittance for Scattered Particles
χ	= Aspect Ratio

I. Introduction

Very low orbits are of great interest for many scientific, civil and military purposes. Recently ESA's mission GOCE ended, it provided detailed information of the Earth's geomagnetic field by orbiting as low as 229 km using ion thrusters to compensate the drag. The amount of propellant on board is a limiting lifetime factor for such a mission, in particular if the S/C is orbiting very low around a planet with atmosphere. The atmosphere is indeed responsible for the drag, which slows down the S/C and reduces its total mission lifetime. It is also a limiting factor in terms of costs, as more drag to be compensated for a longer time means an increased amount of propellant to be carried on board, which again increases the total mass. The lifetime of a S/C orbiting in LEO can be significantly increased by the application of an efficient propulsion system capable to compensate the drag.
The basic idea of an Air-Breathing Electric Propulsion System, shortened RAM-EP, is to use the air of the residual atmosphere as propellant and to process it through a device for generating thrust. This will decrease, ideally nullify, the on board propellant requirement and will generate thrust to partially or fully compensate the drag. A conceptual scheme of the S/C is shown in Fig. 1.

This paper will focus on the device needed to efficiently collect and drive the atmosphere particles to

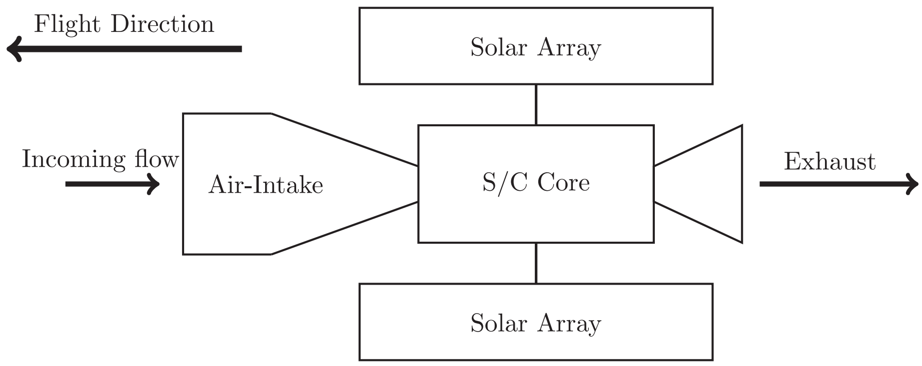

Figure 1: Air-Breathing Electric Propulsion S/C Concept.

the thruster, called the Air-Intake. The investigation on an Air-Intake is part of a Ph.D. program at IRS, focused on the use of a small inductively heated plasma thruster based on IPG6-S for an Air-Breathing Electric Propulsion application,[14].[13] Emphasizing its crucial design, recent studies involved ESA,[4] BUSEK Inc.[8] and JAXA,[5],[7] that proposed and studied different possible design configurations. The outcome of these studies are sustained by DSMC simulations and experimental activity on ground. In the following, an overview of these designs is provided, together with results of DSMC simulations, performed with our in-house code PICLas.[10] Additionally, a simple analytical model based on transmittances and the balance of particle flows is derived, applicable for the analysis and further possible optimization of a generic Air-Intake design. The model is compared to the results of the DSMC simulations and a sensitivity analysis of the basic parameters is performed.

II. Assumptions and Considerations

The design of an Air-Intake for an Air-Breathing Electric Propulsion System is a challenge and depends on many different factors. The requirement is an efficient collection of the particles encountered by the S/C in order to feed the thruster. The ratio between the collected particle flow $\dot{N}_{thr}$ and the incoming particle flow $\dot{N}_{in}$ is named Collection Efficiency, see Eq. 1. In order to have a highly efficient device, it is required to keep η_c as high as possible.

$$\eta_c = \frac{\dot{N}_{thr}}{\dot{N}_{in}} \tag{1}$$

A consideration on the need of an Air-Intake should not be avoided. The flow the Air-Intake encounters will be highly rarefied and, therefore, it is not possible to follow intuition, which is strictly connected to our experience on Earth where continuum flow sovereigns. For different flow conditions, the presence of an

Air-Intake that works perfectly in continuum might worsen and even become counterproductive, providing to the thruster less particle flow than without an Air-Intake. The incoming particle flow to the intake is defined by the open front area of the intake A_{in} and the free stream conditions (e.g. number density n_{in} and velocity v_{in}) as:

$$\dot{N}_{in} = n_{in} v_{in} A_{in} \quad (2)$$

Multiplying the particle flow $\dot{N}$ with the average particle mass m_p results in the corresponding mass flow $\dot{m} = m_p \dot{N}$. With the assumption that the entire collected mass flow $\dot{m}_{thr}$ is accelerated by the thruster, the produced thrust can be calculated as in Eq. 3:

$$F = m_p \dot{N}_{thr} v_{out} = m_p \eta_c \dot{N}_{in} v_{out} = (m_p n_{in} v_{in} v_{out})(\eta_c A_{in}) \quad (3)$$

Here, v_{out} is the exhaust velocity out of the thruster. A deeper description of the influencing factors for the flow into the propulsion device will be further described as part of the balancing model in Sec. IV. In the context of the design of an Air-Intake for an Air-Breathing Electric Propulsion System two important points have to be considered. On the one hand, for maximizing the thrust, not only the efficiency of the thruster itself has to be taken care of, but also a sufficient amount of mass flow has to be provided. Eq. 3 suggests that the area of the intake A_{in} should be as large as possible to collect the most amount of mass flow, however, the S/C front area also determines the drag. On the other hand, when considering the feeding system to the chamber as part of the Air-Intake, the collected gas has also to be fed at a sufficient pressure and, inside an ionization chamber, the neutral gas should remain as long as possible for an efficient ionization process. For this, the particles have to be slowed down while increasing pressure. Therefore, a direct flow of free stream particles into the chamber would not be desired.

III. Air-Intake Review

A. Basic Concepts

The basic concepts for an Air-Intake design are hereby described and shown.
A first logical configuration can be a short cylinder with the cross section of the entire S/C, followed by a simple entrance cone as shown in Fig. 2a. The cross section cone could converge directly to the size of the propulsion system or, alternatively, to a feeding system allowing the other S/C subsystems to be placed behind the Air-Intake.

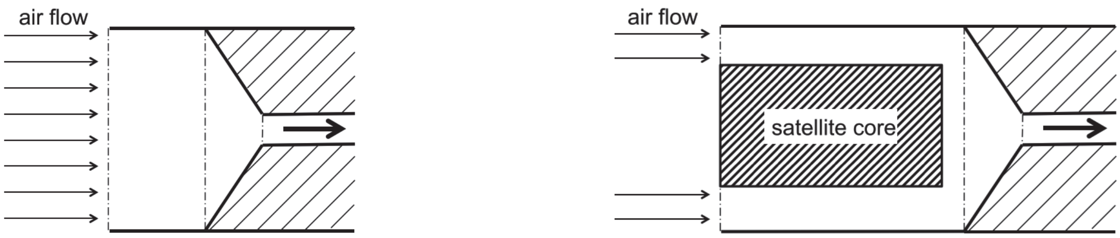

(a) Air-Intake Simple Cone Concept. (b) Air-Intake By-Pass Concept.

Figure 2: Air-Intake Concepts

However, the approach of using a simple cone is not the best one as the flow is not in the continuum regime and, thus, dominated by collisions with the walls rather than of inter-particle collisions. This basically prevents the particles from reaching the end of the cone, which has also been verified through preliminary Direct Monte Carlo Simulations (DSMC), emphasizing the importance of the right wall model. In case of diffusive reflections (the most realistic case[1]), most of the particles will be scattered into a random direction when hitting the wall. As the solid angle including the cone exit represents for the most reflections only a very small part of the entire half space, that comprises all possible target directions, nearly all particles are reflected back into the flight direction. In the case of specular reflection, the situation might be only improved together with a small cone angle. The basic problem arises that the short cylinder between the front collection area and the cone does not have only a high transmission probability for the incoming particles, but also for the flow that is scattered back (the backflow) and, basically, only the particles which

were already directed into the projection of the thruster entrance section will enter into it, resulting in a low collection efficiency η_c.
The performance of the Air-Intake can be improved by providing a design with a high transmission probability for the incoming flow, and trapping it by a lower transmission probability for the backflow. The key concept is that the free stream condition has the nature of being a collimated, hyperthermal flow, as the velocity of the S/C is large compared to the thermal movement of the atmosphere according to the kinetic theory of gases. Thus, it is less obstructed by lateral structures, such as grids or tubes, than the scattered backflow is, which has only thermal movement when diffusive reflections at the walls are assumed. Based on this, a long duct instead of a short one can be better for the collection. According to the study of BUSEK,[8] particles will impact at the end of a long duct on the inclined walls gaining random velocity and, due to the already existing compression, they might be subjected to collisions with the further incoming particles, creating an even higher compression at the end of the duct. The actual influence of this "collision cascade" will be analyzed as part of the DSMC simulation in Sec. V. The difference in the transmission for inflow and scattered backflow might be utilized more efficiently with the introduction of a honeycomb structure of small straws at the entrance of the Air-Intake.
Another configuration is the by-pass design, see Fig. 2b, which can be additionally combined with the honeycomb approach. The flow enters from a ring and reaches the inclined surfaces at the end of the duct. These will act as reflectors/diffusers for the particles which will be then subjected to multiple reflections due to the presence of the satellite core, as shown in the Fig. 2b. The satellite core provides a sensible position for most of the other S/C subsystems.

B. Literature Review

From literature review the most detailed Air-Intake studies for Air-Breathing Electric Propulsion applications are those from ESA,[4] BUSEK[8] and JAXA.[5]

1. *ESA*

The study from ESA[4] considers a mechanical Air-Intake as shown in Fig. 3: At the inlet section, a grid is positioned to stop the incoming particles, a long duct is following to get the required steady pressure level at the end of the device, where a cone shape finally drives particles into the gridded ion thruster GIT. There are important considerations about the fact that over a certain length of the Air-Intake, there is no more improvement in the pressure at the end and, moreover, that a concave or divergent shape at the end does not improve the flow.

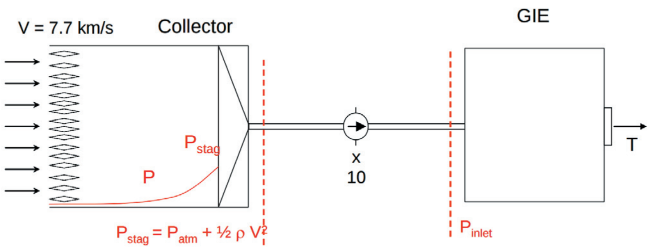

Figure 3: Air-Intake and GIT from ESA.[4]

2. *BUSEK*

The BUSEK Inc.[8] studied the MArs Breathing Hall Effect Thruster (MABHET), a S/C with an Atmosphere-Breathing Electric Propulsion System. In this design, the Air-Intake is a long tube of 3.7 m length and 0.6 m diameter, possibly with a honeycomb structure in the front composed of many straws as described in Sec. A. The Air-Intake is designed as a long tube in order to achieve a higher density region at the back part due to the presence of an assumed "collision cascade". A total pressure increment of 100 was observed in DSMC.

Examplary designs are shown in Fig. 4a and Fig. 4b.

The design of the Air-Intake led to the following observations:

- A long duct allows a compression zone to form at the back, due to collisions between incoming and already trapped particles ("collision cascade");
- Straws fill the inlet, with a certain length, placed in order to block the reflected backflow;
- Main influencing parameter is the ratio of the collisional mean free path to the tube dimension;
- Small inclination of the Air-Intake surfaces will more likely lead to specular reflections at the wall, as the parallel component of the velocity is still much higher than the perpendicular.

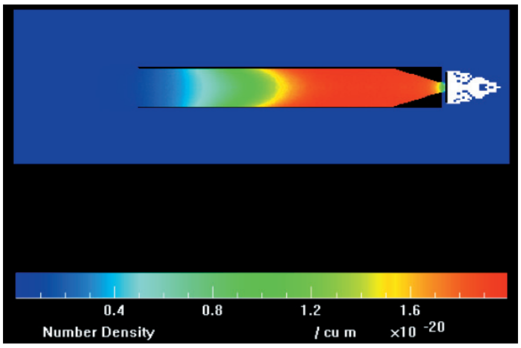

(a) Air-Intake, DSMC results from BUSEK Report.[8]

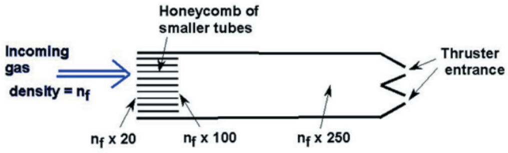

(b) Air-Intake, general concept from BUSEK Presentation.[9]

Figure 4: BUSEK Design

3. Fujita, JAXA

Fujita's study[5] considers a by-pass-like design in which the air flow enters through a ring as shown in Fig. 5. The particles reach the back of the intake hitting a 45° steep surface, the diffuser/reflector, and are afterwards reflected on the back of the satellite core and to the thruster's acceleration grids. Again, such an annular intake represents a structure with different transmission probabilities for the inflow and the backflow, when the effective diameter of the open cross section is small compared to the length. An ECR device ionizes the particles in the part behind the satellite core (the ionization chamber) that are afterwards extracted through accelerating grids. As difference to the BUSEK design, grids are at the outlet, and the whole thruster is already included in the design and, therefore, it is not possible to precisely distinguish between Air-Intake and thruster. In 2012 a new paper from JAXA[7] dealing with the development of this Air-Intake has been published. The main design of the Air-Intake is kept with one important modification, that is the addition of straws inside the ring-shaped inlet region, similarly to the BUSEK design.

From this brief review, the following main points can be summarized:

- A long, annular inlet duct will allow compression at the end of the intake;
- Straws at the entrance section let incoming particles going through, but block the backflow;
- A conical shape at the end of the intake can drive the flow and scatter the particles into the end of the inlet where they can be driven by other matters to the thruster.

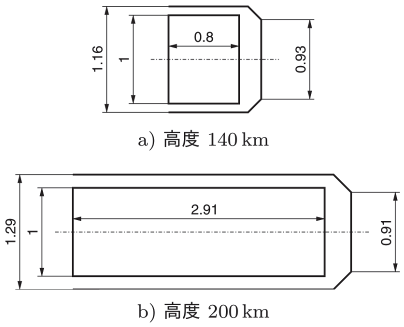

Figure 5: Air-Intake from Fujita's 2004 paper,.[5]

IV. Balancing Model

A. Introduction

In this Section a simple, analytical model for the evaluation of a generic RAM-EP Air-Intake configuration is presented. The generic design becomes obvious when comparing the introduced designs, where an intake section collects the particles with free stream conditions and guides them into the propulsion system. In the context of this model, the intake section is followed by a chamber section in which it is assumed that all particles have already gone through wall collisions and, thus, have only a thermal movement with regard to the wall temperature left. By this, the only particle flows directed out of the chamber are due to thermal diffusion. One flow back through the intake with its desirably low transmittance probability, and another flow through the outlet. The representation of the outlet flow strongly depends on the specific configuration. For the JAXA's design, it is the flow passing through the thruster grids, increased by the acceleration provided by them. In general, a feeding system and the thruster itself follows. By balancing these particle flows, the conditions in the separate sections can be estimated.

B. Assumptions

The basic assumptions for the analytical model are following the nomenclature in Fig. 6:

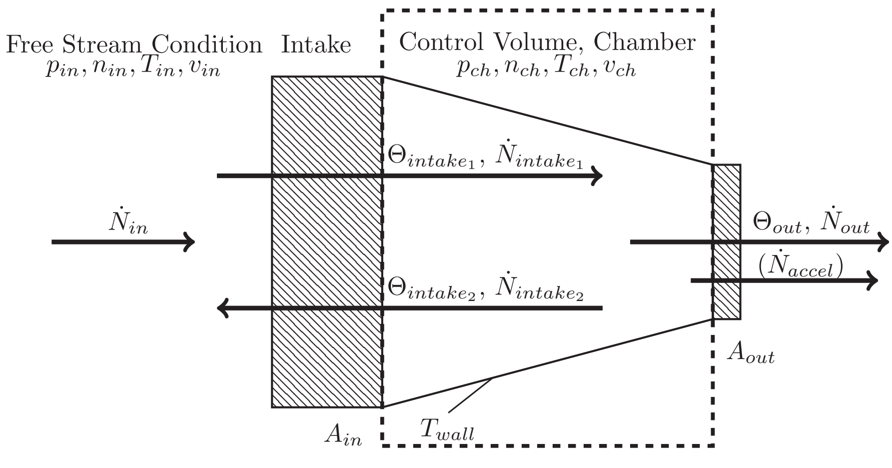

Figure 6: Balancing Model Scheme.

A_{in} and A_{out} are the respective cross sections for the inflow and the outflow representing those of the chamber section. The parameters of the incoming flow are known: number density n_{in} (or pressure p_{in}), flow temperature T_{in} and free stream velocity v_{in}.
Θ is the transmittance into a specific direction through a single structure, indicated in the subscript, and is the fraction of particles which pass through the exit section against the amount of particles which passed

into inflow direction through its start section, as part of them is partially scattered back while crossing the volume. The transmittance can represent any intake, including a case with straws. This is also used for the outlet, for the JAXA case with a transmittance for the acceleration grids. For a general design, it represents the feeding system and thruster.
All in all, three transmittances are to be set: one for the incoming flow, one for the backflow coming from the chamber (accounting for two values through the intake part), and a third for the flow through the outlet. Based on these transmittances, the respective particle flows can be defined. $\dot{N}_{intake_1}$ is the flow of particles passing through the intake section from free stream into the chamber section, $\dot{N}_{intake_2}$ is the backflow that goes back to the free stream after having reached the chamber section, and $\dot{N}_{out}$ is the net outflow.

The basic hypotheses of this model are the following:

- Free molecular flow;
- Single species;
- Ideal gas;
- Complete diffusive accommodation, $\alpha = 1$;
- Fixed temperature, $T_{ch} = T_{wall}$;
- No macroscopic velocity inside the chamber, $v_{ch} = 0\,\mathrm{m/s}$.

The general particle flow into the direction of x_i is defined as in Eq. 4, where n is the number density, $\bar{v}_{x_i}$ is the averaged flow velocity into x_i and A is the passed area perpendicular to $\bar{v}_{x_i}$.

$$\dot{N}_{x_i} = n\bar{v}_{x_i}A \tag{4}$$

Relying on this equation, the particle flow $\dot{N}_{in}$ into the Air-Intake which can be collected at most is simply the one using the free stream conditions and the open area.
Regarding the actually collected flow, the following can be written:

$$\dot{N}_{intake_1} = \dot{N}_{in}\Theta_{intake_1} \tag{5}$$

Based on the for-mentioned hypotheses, the macroscopic velocity of the collected particles will be brought to zero and a superposed backflow will not influence the inflow as it is a free molecular flow.
Starting from the temperature of the particles inside the chamber, the thermal mass flux Γ, defined in Eq. 6, according to [1, p.151], can be calculated.

$$\Gamma(n,T)_{x_i} = n\sqrt{\frac{m_p k_B T_{ch}}{2\pi}} = m_p n \bar{v}_{x_i} \tag{6}$$

Therefore, it is possible to apply Γ to determine backflow and outflow in the chamber of the Air-Intake as following:

$$\dot{N}_{intake_2} = \frac{\Gamma(n_{ch}, T_{ch})}{m_p} A_{in}\Theta_{intake_2} \tag{7}$$

$$\dot{N}_{out} = \frac{\Gamma(n_{ch}, T_{ch})}{m_p} A_{out}\Theta_{out} + \dot{N}_{accel} \tag{8}$$

To this, the continuity equation, see Eq. 9, can be applied which states that the net particle flow through a control volume, in this case the chamber section, having certain number of outlets and inlets must be zero. $\dot{N}_{accel}$ is the accelerated particle flow which will be actively extracted by the thruster. This value strongly depends on the operation point of the specific thruster and its respective acceleration process and is, amongst others, also a function of the n inside the chamber. It is expected that a minimum n is needed inside the chamber for the thruster ignition. Therefore, the focus is at the situation before ignition, $\dot{N}_{accel} = 0$.

$$\dot{N}_{intake_1} = \dot{N}_{intake_2} + \dot{N}_{out} \tag{9}$$

The assumption of a nullified macroscopic velocity in the chamber allows to rewrite Eq. 9 as in Eq. 10:

$$\dot{N}_{in}\Theta_{intake_1} = \frac{\Gamma(n_{ch}, T_{ch})}{m_p}(A_{in}\Theta_{intake2} + A_{out}\Theta_{out}) \tag{10}$$

Therefore Γ can be extracted and, thus, the density n_{ch} inside the chamber from Eq. 6 results in:

$$n_{ch} = \Gamma(n_{ch}, T_{ch})\sqrt{\frac{2\pi}{m_p k_B T_{ch}}} \tag{11}$$

The pressure can be calculated by applying the ideal gas condition as:

$$p_{ch} = n_{ch} k_B T_{ch} \tag{12}$$

It is therefore possible to analytically calculate the parameters inside the chamber section, when input conditions and transmittances are given. Based on this, efficiencies for the number particle flow, pressure and mass flow can be extracted. The approach will be verified through DSMC simulation in Sec. V.
The number density inside the chamber is the value which results together with the other gas properties in a thermal effusion out of the chamber equal to $\dot{N}_{intake_2}$ and the effusion part of $\dot{N}_{out}$. In a dynamic view, this values rises until the balance is reached. Considering also the extracted flow $\dot{N}_{accel}$, it is expected that the actual n_{ch} will decrease after ignition, since the thermal effusion required for mass balance would be smaller. Collection Efficiency η_c in Eq. 13, pressure ratio in Eq. 14 and number density ratio in Eq. 15 are important values for the evaluation of an Air-Intake. With regard to Eq. 1, $\dot{N}_{thr}$ can be seen either as $\dot{N}_{intake_1}$ or as $\dot{N}_{out}$. For consistency with the respective publications of the analyzed designs and for a simple comparison with the DSMC simulations, the latter has been chosen.

$$\eta_c = \frac{\dot{N}_{out}}{\dot{N}_{in}} = \frac{\Gamma(n_{ch}, T_{ch})}{m_p}\frac{A_{out}\Theta_{out}}{\dot{N}_{in}} = \frac{\Theta_{intake1}A_{out}\Theta_{out}}{A_{in}\Theta_{intake2} + A_{out}\Theta_{out}} \tag{13}$$

$$\frac{p_{ch}}{p_{in}} = \frac{m_p\dot{N}_{in}\Theta_{intake1}}{A_{in}\Theta_{intake2} + A_{out}\Theta_{out}}\sqrt{\frac{2\pi}{m_p k_B T_{ch}}}\frac{T_{ch}}{T_{in}n_{in}} \tag{14}$$

$$\frac{n_{ch}}{n_{in}} = \frac{m_p\dot{N}_{in}\Theta_{intake1}}{A_{in}\Theta_{intake2} + A_{out}\Theta_{out}}\sqrt{\frac{2\pi}{m_p k_B T_{ch}}}\frac{1}{n_{in}} \tag{15}$$

V. Air-Intake Simulations

In this section, the DSMC simulations performed with our in-house code PICLas are presented. The consideration of a honeycomb structure of small straws at the entrance required an elaborate modelling approach which is additionally described.

A. PICLas

PICLas, developed at the IRS and the Institute of Aerodynamics and Gas Dynamics (IAG) of the University of Stuttgart,[10] was employed for the following simulations. The code is a coupled, three-dimensional particle method based on unstructured, hexahedral meshes and includes, besides general routines for particle tracking and particle-wall collisions, a Direct Simulation Monte Carlo (DSMC)[1] as well as a particle-in-cell method, with additional modules for Low Diffusion and Fokker-Planck models.[11]
In the context of this paper, only the DSMC part was used. A pairing scheme including the Natural-Sample-Size method with the variable hard sphere model was applied for inter-particle collisions. Internal degrees of freedom of molecules were taken into account while neglecting chemical reactions because of the relatively low temperatures in all simulations. By switching the pairing scheme off (corresponding to collision probabilities of zero) and, thus, using only the tracking, wall collisions and analysis routines, also ideal, free molecular flows were simulated.
In general, symmetry was exploited by simulating only one quarter of the domain. Diffusive reflection with

full accommodation was assumed at walls, whereas specular reflection for the planes of symmetry. All other boundaries were open with a defined transparence (i.e., crossing particles are deleted with the given probability, otherwise reflected) with an optional inflow from a virtual buffer layer filled with particles of a Maxwell-Boltzmann distribution corresponding to the respective inlet condition.

B. DSMC Simulations of the Reference Cases

1. JAXA Air-Intake

Based on the Fujita's 2004 study,[5] DSMC simulations have been performed for comparison with their paper results and to verify the balancing model. The input values are the same as reported in the paper[5] (atmospheric model MSISE-90), as well as the geometrical data. In particular, two different geometric configurations are considered, with a form factor of $\chi = 10.0$ for a short intake optimized for low altitudes, and $\chi = 20.0$ for a longer intake optimized for higher altitudes. The form factor χ, see Fig. 7, is defined as in Eq. 16. Two altitudes have been simulated, 140 km and 180 km, the highest with both geometries ($\chi = 10.0$ and $\chi = 20.0$) and the lowest with a different outlet transmittance, given by the acceleration grids of the assumed thruster ($\Theta_{out} = 0.1$ and $\Theta_{out} = 0.2$).[5]

$$\chi = \frac{L_1}{R_2 - R_1} \tag{16}$$

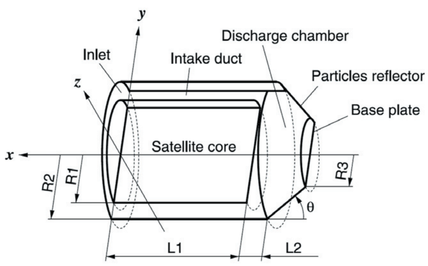

Figure 7: Air-Intake Geometry,.[5]

Additionally to the MSISE-90, the NRLMSISE-00 atmosphere model was used for comparison. It is the most advanced regarding the composition of the atmosphere at low altitudes.[12] The differences of the two models are, in our simulations, the inclusion of additional species (He and Ar at 140 km, also N at 180 km), a lower T_{in} and a slightly lower n_{tot}. Input parameters for the model have been set for 01/01/2014 at $hour = 1.50$, lat. 55.00, long. 45.00 in average solar and geomagnetic activity defined by $F10.7 = F10.7_{avg} = 140$ and $Ap = 15$. In Tab. A1 of the Appendix the input parameters are shown.
Concerning the short Air-Intake, $\chi = 10.0$ at 140 km using NRLMSISE-00 model, DSMC simulations have been run also with the hypothesis of an ideal free molecular flow, that means considering only collisions between particles and walls. By this, the contribution, if there is any, of inter-particle collisions inside the chamber can be evaluated.

The results of our simulations are compared to the Fujita's from 2004 in Tab. 1 in terms of the averaged value of the total number density n inside the region behind the satellite core. Results have, except for the $\chi = 10$ case at 180 km, a deviation of less than 10% from the reference values. Therefore the results are, at least, in the same range and verify the general simulation set-up. The main reason of the deviations is assumed to be the ambiguity of a defined chamber pressure. Furthermore, not all assumptions of the reference are known.
A more elaborate presentation and discussion of the results is given in Sec. VI.

2. BUSEK Air-Intake Simulation

Based on the BUSEK design,[8] DSMC simulations have been performed to cover a wider range of Air-Intake configurations. The considered design is supposed to operate in a low Mars orbit and is a 3.7 m long tube

Table 1: Fujita's 2004 Air-Intake DSMC Results Comparison

h	χ	Θ_{out}	n_{ch}, from[5]	$n_{avg,ch}$, PICLas	Rel. Dev.	Note
km	-	-	m^{-3}	m^{-3}	%	-
140	10.0	0.1	7.24×10^{18}	7.77×10^{18}	$+7.32$	
140	10.0	0.2	4.82×10^{18}	4.95×10^{18}	$+2.70$	
"	"	"	"	4.40×10^{18}	-8.71	NRLMSISE-00
180	10.0	0.2	1.11×10^{18}	9.32×10^{17}	-16.04	
180	20.0	0.2	1.37×10^{18}	1.237×10^{18}	-9.71	
"	"	"	"	1.01×10^{18}	-26.28	NRLMSISE-00

Table 2: BUSEK Air-Intake DSMC Results Comparison

η_c, from[8]	η_c, PICLas	Rel. Dev.	Note
%	%	%	-
28	23	-17.9	With Collisions
< 19	17	-	No Collisions
"	20	-	With Straws, With Collisions
< 19	15	-	With Straws, No Collisions

with a 0.6 m diameter terminating with a conical surface converging on a 0.14 m diameter exit to fed the Hall-Thruster. As complete data is not available, n has been extracted from a given plot showing the compression efficiency η_c at different products of number densities and intake diameter. A value of $n_{tot} = 5.3 \times 10^{17}\,\mathrm{m}^{-3}$ was used for the simulated intake diameter of 0.6 m. Remaining flow condition are set to $v_{in} = 3.5\,\mathrm{km/s}$ and $T_{in} = 250\,\mathrm{K}$, the latter represents a common value for the temperature of the upper Mars atmosphere.[6] As simplifying assumption only CO_2 was considered (that is present $\sim 96\%$) and the internal degrees of freedom of the particles were neglected.

The main physical principle pointed out by BUSEK is the pushing of the incoming particles on the already trapped particles by inter-particle collisions. To quantify this effect, those collisions have been switched off for comparison, analogously to the JAXA cases. The main results from the simulations are briefly presented in Tab. 2 and compared to the available data from BUSEK,[8] that is an η_c of $\sim 28\%$ for the simulated point and $\sim 19\%$ for the lowest included n which is, therefore, interpretable as an upper limit for the simulations assuming free molecular flow. The results are here also in the same range as those from the reference which verifies the general system set-up, but emphasizes the availability lack of the exact reference assumptions. In Tab. 2 there also already simulations with included straws, these will be further described in Sec. VI.

C. Consideration of Straws inside the Air-Intake

JAXA[7] and BUSEK[9] presented an Air-Intake with a honeycomb straw structure inside the inlet. The function of the straws, as already explained, is to minimize the backflow and, therefore, increase pressure and density at the end of the Air-Intake and η_c. The main assumption for the straws, in both studies, is that the incoming flow, as result of being hyperthermal, is well collimated and no interaction between particles and straw walls will arise. That means the particles will keep their macroscopic velocity until they scatter at the surfaces of the end of the Air-Intake.

1. Implementation in DSMC

Due to the high computational resources required for the actual inclusion of an honeycomb straw structure into the DSMC domain, a simplifying modeling approach has been used within the simulations.

For this, single straws have been simulated, represented by simple cylinders open at both sides with an incoming flow along the direction of the axis. To simulate the Air-Intake completely with straws, the velocity

distribution at the outlet of a single straw has been extracted and used as input for the Air-Intake simulation itself. The velocity distributions show two main peaks, one corresponding to the high, macroscopic velocity of particles that went through the straw without wall collisions, and another for the particles scattered along the inner wall, with a macroscopic velocity of zero. The number of fast and of scattered particles are extracted from the simulations and the respective transmittances, Θ_{fast} and $\Theta_{scattered}$, used for the following Air-Intake simulations were included.
As there will be also a backflow from the downstream part of the intake through the straw, a transmittance for this flow is needed. The corresponding problem is an already well-known subject of gas kinetics, mostly connected to the work of Clausing[2] who dealt with free molecular flow through cylinders in terms of transmission probability. The Clausing Factor, referred as $\Theta_{Clausing}$, depends only on the L/R ratio of the respective cylinder and is valid under the following assumptions:

- Ideal free molecular flow;
- $v_{in} = 0$;
- $T_{in} = T_{wall}$;
- fully diffusive reflections at the walls, $\alpha = 0$.

Precise solutions of the Clausing equations were calculated by Cole[3] for discrete L/R ratios. These solutions were used, rather than the long tube approximation, in which the Clausing factor is approximated as in Eq. 17, due to the significant error the latter produces in the range of our interest ($L/R < 100$), as shown in Fig. 8. For example, the relative error is $\sim 40\%$ for $L/R = 10$ and still of 5% for $L/R = 100$.

$$\Theta_{Clausing} = \frac{8}{3}\frac{R}{L} \tag{17}$$

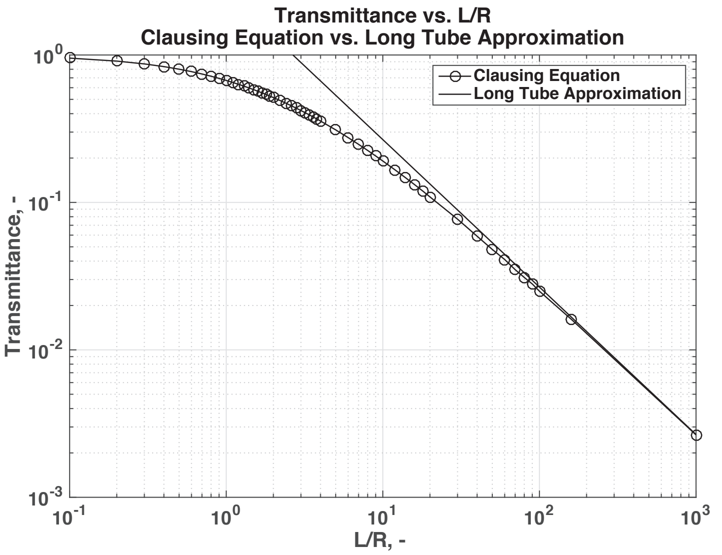

Figure 8: Comparison of Precise Clausing Factors Against Long Tube Approximation.

2. Verification of the Approach

To verify the applicability of the for-mentioned approach for the inclusion of straws into the Air-Intakes simulation, additional DSMC simulations have been performed for a geometry including only the annular intake section of Fujita's Air-Intake, by which, the required transmittances could be extracted for a simulation including only the part after the satellite core. This has been chosen as the effective diameter of the ring open cross section is small compared to the length, similarly as for a single straw and, thus, it shows a similar

compression ability. Furthermore, the general approach can be demonstrated in the following.
The intake section to be modeled is simulated with open boundaries at both ends, i.e., all particles crossing these areas are deleted. However, their velocities during the crossing are saved, which enables the evaluation of the velocity distribution. This probability density function of directed velocity,however, does not represent the function inside a given volume, as every particle crossing an outlet was saved and, therefore, fast particles were preferred against slow velocities which could have started also from a larger distance. The velocity distribution at the end is assumed to be Bi-Maxwellian, including the fast, unscattered particles with v_{in} and T_{in} on the one hand, and the scattered particles with T_{wall} on the other hand. Based on this, the only values to be extracted are the flow rates of fast and scattered particles that flow into the domain. These are the corresponding transmittances Θ_{fast} and $\Theta_{scattered}$ multiplied by the incoming particle flow. An accepted error is based on the fact that particles with a large lateral velocity will be scattered inside the cylinder with a higher probability and, thus, the outflow is not supposed to follow an ideal, Gaussian distribution into those corresponding directions.
Fig. 9 shows the corresponding data for the simulated case including both inlet and outlet section. A, B and C are the areas given by the integrals over the individual distributions, respectively of the scattered backflow A, the scattered flow B and the fast/unscattered flow C. As the sum of all 3 areas $(A + B + C)$ represents N_{in}, Θ_{fast} is calculated as $C/(A + B + C)$ and $\Theta_{scattered}$ as $B/(A + B + C)$. The same was conducted for an inflow without macroscopic velocity, giving only the areas A and B and a $\Theta_{Clausing}$ of $B/(A+B)$. These three transmittances, shown in Tab. 3, were applied as input to the simulation including only the chamber section as mentioned above. Results showed no significant difference to the simulation including both intake and chamber section, as it will be shown in Sec. VI. Therefore, the extraction of the approach has been verified and can be applied for the straw implementation.

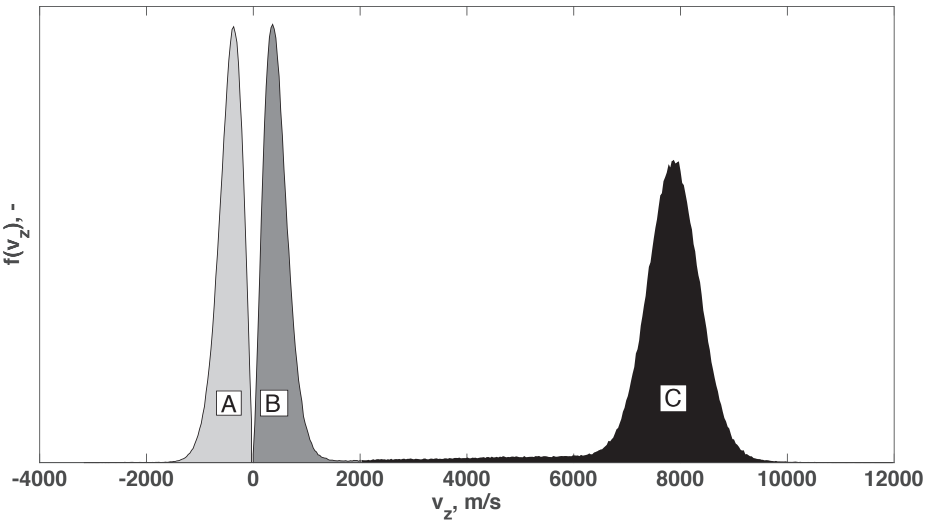

Figure 9: Extracted Velocity Distribution, Fujita's design inflow including only the Annular Intake Section.

Table 3: Annular Intake Section Transmittances.

El.	$\Theta_{Clausing}$,(A)	$\Theta_{scattered}$,(B)	Θ_{fast},(C)
O	0.212	0.289	0.392
N_2	0.212	0.276	0.466
O_2	0.212	0.253	0.512

3. *JAXA Straws*

In 2012 a new paper from JAXA[7] dealt with the improvement of Fujita's design, in particular a model for laboratory testing was developed with the addition of straws in a honeycomb structure, and tested with an atomic oxygen flux generator. Since the geometry of this particular Air-Intake is not available, its straws with a $L/R = 20$ have been applied to the Fujita's design for the altitude of 140 km, $\chi = 10$. The atmospheric model applied is the NRLMSISE-00. The transmittances extracted from our simulations are summarized for each species in Tab. 4.

Table 4: JAXA Straw Transmittances Results.

Element	Θ_{fast}	$\Theta_{scattered}$	$\Theta_{Clausing}$
Ar	0.381	0.293	0.109
He	0.064	0.288	0.109
N_2	0.307	0.315	0.109
O	0.204	0.334	0.109
O_2	0.333	0.308	0.109

4. *BUSEK Straws*

In the BUSEK presentation on MABHET,[9] straws are mentioned to be used in the Air-Intake for the forementioned reasons. Detailed information on their geometry is not available and, therefore, a rough estimation from the schemes in the report[8] and in the presentation[9] was done. The estimated values provide an aspect ratio of $L/R \sim 35$. The extracted transmittances are presented in Tab. 5.

Table 5: BUSEK Straw Transmittances Results.

Element	Θ_{fast}	$\Theta_{scattered}$	$\Theta_{Clausing}$
CO_2	0.100	0.306	0.067

VI. Simulation Results and discussion

In this section, the results of the Air-Intake simulations for both Fujita/JAXA and BUSEK cases, also with the inclusion of straws, are presented and discussed. Averaged, macroscopic values inside discrete cells are extracted for the total number density n and velocity v_z into inflow direction z from lines along the Air-Intake, as it is shown in Fig. 10 together with contours of total n for the JAXA intake with MSISE-90 model, $\chi = 10.0$ and $\Theta_{out} = 0.2$ at 140 km ("chamber" illustrates the averaging volume for the calculation of n_{ch}). For the BUSEK cases, center lines have been extracted.

A. JAXA Air-Intake

Fig. A1a in the appendix, shows v_z and n along the intake for the reference cases at 140 km. n increases when getting closer to the chamber while the v_z decreases, which is also expected as the part of scattered particles increases. Higher density and lower velocity are shown in the case with a lower transmittance of the outlet grid, indicating a higher compression. In the plot the result including only the chamber section for the modeling of the velocity distribution is also shown, and very good agreement is visible, therefore, verifying the extraction approach of the velocity distribution.
Fig. A1b shows the results for the Air-Intake at 180 km with both atmospheric models and both χ. Red and black lines are using the same atmospheric model but a different χ, the short Air-Intake optimized for 140 km provides indeed a smaller n while keeping the velocity higher than in the case with the long Air-Intake of $\chi = 20.0$. The slightly lower n of the NRLMSISE-00 model compared to the MSISE-90, produces the lower n in the Air-Intake of the same size, the different T_{in} probably influences the shape of the curve itself. Tab. 6

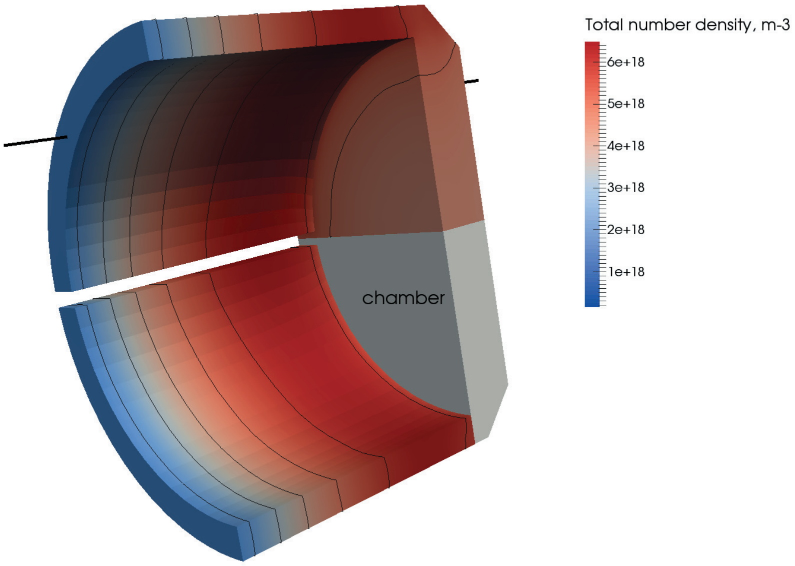

Figure 10: JAXA intake with MSISE-90 model, $\chi = 10.0$ and $\Theta_{out} = 0.2$ at 140 km.

shows the results of the simulations performed with the NRLMSISE-00 model, illustrating the influence of inter-particle collisions and straws inside the intake. In particular, the extracted average number density over the chamber volume $n_{avg,ch}$ is shown. Starting from this value the pressure and density ratio are derived and, moreover, η_c is also included. The line plots of the Air-Intake are shown in Fig. A2 in the Appendix. Results indicate that the use of straws, in this particular geometric configuration, will provide less n in the chamber, thus, density and pressure ratio and, therefore, also η_c will be lower. In particular, from Fig. A2, the n profile shows an higher value at the entrance, which decreases towards the chamber. The opposite behavior is obtained without straws which shows the additional compression by the straws but, as a matter of fact, only at the inflow part of the intake. Lower performance of the Air-Intake means that the presence of straws is counterproductive for this particular geometry. Regarding the effect of the inter-particle collisions in the case without straws, both simulations have very similar results which shows the good approximation of an ideal free molecular flow for this specific case. With collisions, a slightly lower n is achieved inside the chamber, possibly due to the fact that the particles represent an obstacle for the incoming flow.

Table 6: DSMC Results for JAXA's design: Influence of inter-particle collisions and straws inside the intake.

h km	χ -	Θ_{out} -	$n_{avg,ch}$ m^{-3}	η_c -	p_{ch}/p_{in} -	n_{ch}/n_{in} -	Note
140	10.0	0.2	4.40×10^{18}	0.49	29.4	56.9	NRLMSISE-00, With Collisions
"	"	"	4.64×10^{18}	0.50	31.0	60.0	NRLMSISE-00, Without Collisions
"	"	"	3.61×10^{18}	0.40	24.1	46.7	NRLMSISE-00, Straws, With Collisions

B. BUSEK

Fig. A3 in the Appendix shows n along the center line (z axis) of the BUSEK Air-Intake design. The rapidly decreasing n at the end of the intake is due to the assumption of a completely open outlet[8] with no backflow. In the real case, the thruster systems would follow, creating also a backflow. The DSMC results of the simulations without straws (black and blue lines) show that n significantly increases and reaches a region of nearly constant state at the back, if collisions are taken into account. When collisions are neglected, that region is missing and, instead, an almost linear increase of n along the Air-Intake occurs with a maximum

less than the maximum value of the case with collisions. This shows that the assumed cascade effect actually exists, in which incoming particles collides with the trapped particles and form a region of higher pressure at the back of the Air-Intake. Concerning the application of straws to this design, Fig. A3 shows a slightly lower n, but based on the higher n in the front part it is evident that particles are actually trapped inside the Air-Intake. Conspicuous is the existence of a region of lower n in front of the honeycomb outlet with increasing n into both direction for the collisional case, while, without collisions, n is monotonically decreasing, similar to the JAXA case with straws. This can be explained by the collisions of incoming particles with the trapped ones, representing an obstacle in the case with collisions. This can be also seen in Fig. A4 that shows the velocity along the z axis. In the cases with collisions, there is a jump in the velocity at the entrance - the particles already inside are pushed into the intake.
All in all, results show that colliding particles will actually create a region of higher n at the back of the Air-Intake, and that this principle can be used to generate a region of higher constant n inside the Air-Intake. However, an actual improvement by the existence of straw cannot be observed which motivated a more detailed analysis of their influence.

VII. Application of the Balancing Model and Straw Sensitivity Analysis

A. Comparison of the Balancing Model with DSMC

In the following, the Balancing Model is verified for exemplary cases analyzed by DSMC. They were:

1. Fujits's design, MSISE-90 model, $\chi = 10.0$ and $\Theta_{out} = 0.2$ at 140 km, with collisions;
2. Fujita's design with NRLMSISE-00 model and straws, with collisions;
3. BUSEK design without straws (with and without collisions);
4. BUSEK design with straws (with and without collisions).

Same inflow conditions as for the DSMC simulations were used. As the transmittances are different for each species, the balancing model was applied for each species and the resulting n and $\dot{N}$ are added together for calculating the total values. The cases with straws represent an intake section including two separate parts - the straws and the remaining intake without straws. Therefore, Eq. 18 is applied for combining two transmittances Θ_A and Θ_B to a single value Θ_{AB}, with A for the straw values and B for the values of the remaining free intake (a ring for the Fujita/JAXA and tube for the BUSEK case).

$$\Theta_{AB} = \Theta_A\Theta_B + \sum_{n=0}^{N} \Theta_A(1-\Theta_B)(1-\Theta_{A,Clausing})[(1-\Theta_{A,Clausing})(1-\Theta_{B,Clausing})]^n \Theta_{B,Clausing} \quad (18)$$

Similar to the straw implementation in DSMC, transmittances were divided into $\Theta_{AB,scattered}$ and $\Theta_{AB,fast}$, their sum was used for the transmittances inside the balance model. The values were taken from DSMC simulations (Θ_B for the JAXA cases from calculations of only the intake ring) or, where applicable, as known Clausing Factors. The transmittances are summarized in Tab. A2 in the Appendix.
As Tab. 7 shows, results agree very well with DSMC results in terms of n_{ch} and η_c. Compared to the DSMC simulations assuming free molecular flow (corresponding to the same conditions as for the Balancing model), the relative error is less than 10%, in the Fujita/JAXA case with straws even nearly exact for n_{ch} and -1.3% regarding η_c. For the BUSEK case, the values are also compared to the simulations without collisions and are still in the same range. Regarding the increased discrepancy when compared to DSMC with collisions, this is because their effect is that the incoming particles literally push the already trapped particles further into the Air-Intake, therefore increasing η_c and n. In the Balancing Model, this cannot be taken into account, as it assumes free molecular flow.
The Balancing Model seems to be a very good approximation for the DSMC results and it also confirms the reduction of η_c when including straws inside the intake section. However, most of the used transmittances have to be calculated by DSMC at first and, thus, this does not represent a general approach for evaluating any arbitrary configuration. For this, the transmittances need to be calculated directly from a given geometry.

Table 7: Results Balancing Model, BM, vs. DSMC Results

Case	n_{ch}^{DSMC} m^{-3}	η_c^{DSMC} %	n_{ch}^{BM} m^{-3}	η_c^{BM} %	Err. n_{ch} %	Err. η_c %
JAXA	4.95×10^{18}	48	5.34×10^{18}	51	+7.9	+5.8
JAXA with straws	3.61×10^{18}	40	3.61×10^{18}	40	0.0	-1.3
BUSEK (without collisions)	$\sim 6.1 \times 10^{19}$	17	6.43×10^{19}	18	+5.4	+4.7
BUSEK (with collisions)	$\sim 7.5 \times 10^{19}$	23	"	"	-14.3	-21.4
BUSEK with straws (without collisions)	$\sim 6.5 \times 10^{19}$	15	5.93×10^{19}	17	-8.8	+7.8
BUSEK with straws (with collisions)	$\sim 6.5 \times 10^{19}$	20	"	"	-8.8	-16.7

B. Straw Sensitivity Analysis

DSMC simulations on various straw geometries with macroscopic $v_{in} > 0$ have shown that a certain fraction of the particles does not collide with the walls and leaves the straw with inflow condition, while the remaining part is scattered, and has only a thermal movement corresponding to T_{wall} left. As this problem is not covered by the well-known Clausing's assumptions and equations, it is of interest to get a wider idea of how straw geometries and flow conditions influence the respective transmittances. Therefore, a sensitivity analysis was performed by DSMC simulations varying the following parameters:

- T_{in} and T_{wall};
- incoming flow velocity, v_{in};
- particle mass m_p, different species;
- L and R.

The results of the sensitivity analysis are shown in Tab. A3 in the Appendix. By comparing Cases 1 and 3, both having the same L/R ratio but different radii, it is expected that for the same ratio, the same Θ's follow. Additionally, Cases 1 and 2 show that if the ratio T_{wall}/m_p is kept constant, the transmittances do not change. Cases 4 and 5, and 10 and 11 illustrate that T_{wall} does not have any influence and Cases 7 and 8 that Θ's do not change for a constant $v_{in}R/L$. All in all, it can be assumed that in the considered range of parameters, the driving non-dimensional value is X from Eq. 19.

$$X = \frac{\sqrt{\frac{k_B T_{in}}{m_p}}}{v_{in}} \frac{L}{R} \tag{19}$$

The ratio of the square-root and v_{in} can be interpreted as the one of the lateral, thermal velocity to the axial, macroscopic velocity. Plotting all points of Tab. A3 in terms of $\Theta(X)$ results in Fig. 11. It can be seen that the transmittances correlate well by the use of the polynomial fits given in Eq. 20 for the scattered part and Eq. 21 for the fast part. Based on this, different values of L/R can now be analyzed both for JAXA and BUSEK cases. L/R values with $\Theta_{Clausing}$ given by Cole[3] were used, in particular the X range was kept the same as for the correlation. The length is kept constant (corresponding to different straw radii) which enables the use of the same transmittances for the remaining intake part without straws (B from Eq. 18).

$$\Theta(X)_{scattered} = \Theta_2 = 0.041447835X^3 - 0.2850944924X^2 + 0.5808664686X - 0.031410537 \tag{20}$$

$$\Theta(X)_{fast} = \Theta_1 = -0.0532264802X^3 + 0.405367838X^2 - 1.0704252233X + 1.0533360985 \tag{21}$$

In Fig. 11 represents Θ_3 the total inflow transmittance, while the Clausing factor $\Theta_{Clausing}$ represents the backflow transmittance. The former depends on both the geometry (L/R) and the inflow conditions (T_{in},m_p and v_{in}), but the latter only on L/R. By merging both dependencies to the single value X, Θ_3 is now dependent on solely X and $\Theta_{Clausing}$ additionally on the geometry or the inflow conditions. Therefore, $\Theta_{Clausing}$ is shown for a set of three different inflow conditions representing most of the range of the sensitivity analysis and, thus, the considered RAM-EP cases. Fig. 11 shows that, independently from the actual flow condition, Θ_3 decreases always slower than $\Theta_{Clausing}$ for low L/R ratios, but faster for large ratios. Therefore, it is preferable to choose a design with low L/R ratios, as an high transmittance for the inflow, together with a low transmittance for the backflow is desired. Moreover, it can be seen that for a fixed X, $\Theta_{Clausing}$ increases with T_{in} and decreases with m_p and v_{in}, while Θ_3 remains constant. By this, it can be assumed that, e.g., lighter species are collected less efficiently than heavier ones, as it is also shown in Fig. A5. Fig. A5, A6, A7, and A8 in the Appendix show the resulting dependence of n_{ch} and η_c from L/R for the separate species of the JAXA case and three different intake lengths for the BUSEK case. They show that, for the considered range of parameters, the Air-Intake is supposed to be most efficient for small L/R, corresponding to a simple grid. To verify this conclusion, DSMC simulations for shorter geometries should be performed which would additionally include the influence of inter-particle collisions.

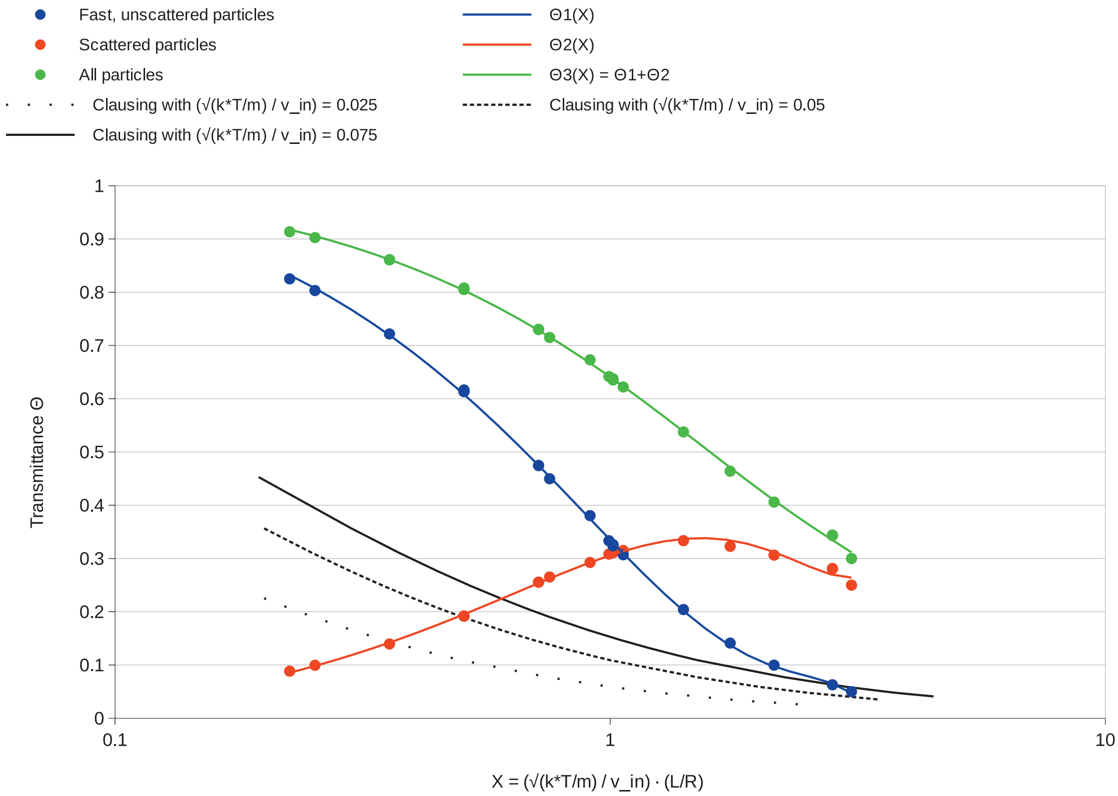

Figure 11: Generalized Cylinder Transmittances

VIII. Conclusion

This paper focused on the Air-Intake which collects and drives the atmosphere particles to the thruster, in an air-breathing electric propulsion system. Recent studies have been reviewed, in particular the focus has been on the Fujita's design, its improvement from JAXA and the BUSEK design. Their early results have been verified through our DSMC code.

Moreover, the introduction of straws and the influence of inter-particle collisions inside the Air-Intake, that could improve the collection efficiencies, have been analyzed. In order to simulate the presence of straws, a method of extraction of the velocity distribution at the end of a single straw to be inserted as input condition for the Air-Intake has been verified and applied.

A sensitivity analysis on the straws in terms of various input parameter has been performed and showed the dependency of the transmittances results. The velocity distribution shows that the particles will always interact with the straw and, therefore, only a part of the flow will reach the end with a macroscopic velocity while the rest will be only moving due to thermal diffusion.

In particular for the Fujita's design, the introduction of the straws of JAXA studies has shown a decrease collection efficiency η_c and a smaller total number density n_{ch} inside the chamber than in the case without. The application of a newer atmospheric model showed slightly lower atmospheric n and lower T_{in}.
Regarding the BUSEK study, the principle of a collision cascade at the end of a long tube shaped Air-Intake that generates a compression has been verified. In particular a cushion of almost constant n is present in front of the end of the Air-Intake and its length is increased by the addition of straws, although with a decrease of n.
A balancing model based on separated particle flows and transmittances has been introduced and compared with the DSMC results which have shown a good approximation in the results, however it must be sustained by the calculation of transmittances a priori. With this model a sensitivity analysis over the L/R ratio of the straws has been performed and applied to Fujita's and BUSEK Air-Intakes.
This was additionally sustained by the development of a correlation between geometry/flow data and the respective transmittance. Ideally, it should be as high as possible for the inflow, and as low as possible for the backflow in an Air-Intake. The results show indeed, that a lower L/R ratio is preferable as it provides higher η_c and n_{ch}. It suggests that a grid, rather than a honeycomb structure of straws at the front of the Air-Intake, shall be used to form a higher performance Air-Intake.

Appendix

Table A1: Inflow Conditions for Fujita/JAXA cases.

h	$n_{tot,in}$ $\times 10^{16}$	T_{in}	v_{in}	n_{N_2} $\times 10^{16}$	n_{O_2} $\times 10^{15}$	n_O $\times 10^{16}$	n_{Ar} $\times 10^{13}$	n_{He} $\times 10^{13}$	n_N $\times 10^{12}$	Atm. Model
km	m^{-3}	K	km/s	m^{-3}	m^{-3}	m^{-3}	m^{-3}	m^{-3}	m^{-3}	-
140	8.73	682.0	7.82	5.68	3.84	2.67	-	-	-	MSISE-90
"	7.73	580.5	7.82	4.36	3.79	2.98	8.68	0.29	-	NRLMSISE-00
180	1.75	968.0	7.80	0.90	0.47	0.80	-	-	-	MSISE-90
"	1.38	731.4	7.80	0.53	0.29	0.815	0.45	4.12	9.30	NRLMSISE-00

Table A2: Balancing Model Results.

Case	Straw			Ring/Tube				
	$\Theta_{scattered}$	Θ_{fast}	$\Theta_{Clausing}$	$\Theta_{scattered}$	Θ_{fast}	$\Theta_{Clausing}$	$\Theta_{intake1}$	$\Theta_{intake2}$
Fujita/JAXA, O	1	1	1	0.289	0.392	0.212	0.681	0.212
", N_2	1	1	1	0.276	0.466	0.212	0.742	0.212
", O_2	1	1	1	0.253	0.512	0.212	0.765	0.212
Fujita/JAXA, O	0.330	0.200	0.109	0.255	0.472	0.222	0.401	0.078
", N_2	0.330	0.200	0.109	0.255	0.472	0.222	0.488	0.078
", O_2	0.310	0.330	0.109	0.202	0.597	0.222	0.500	0.078
", He	0.290	0.064	0.109	0.243	0.265	0.222	0.256	0.078
", Ar	0.290	0.38	0.109	0.182	0.642	0.222	0.533	0.078
BUSEK	1	1	1	0.265	0.447	0.162	0.712	0.162
"	0.307	0.099	0.067	0.240	0.507	0.181	0.315	0.049

Table A3: Extracted Straws Transmittances from DSMC Simulations.

Case No.	L/R -	v_{in} km/s	T_{wall} K	T_{in} K	m_p /El. $\times 10^{-26}$ kg	Θ_{fast} -	$\Theta_{scattered}$ -	Note
1	10	7.80	300	300	2.66/O	0.613	0.192	$R = R_1$
2	10	7.80	600	600	$5.31/2 \times$ O	0.613	0.192	
3	10	7.80	300	300	2.66/O	0.616	0.192	$R = R_1/2$
4	10	7.80	150	150	2.66/O	0.722	0.139	
5	10	7.80	600	150	2.66/O	0.721	0.139	
6	10	15.60	300	300	2.66/O	0.803	0.099	
7	10	3.90	300	300	2.66/O	0.326	0.311	
8	20	7.80	300	300	2.66/O	0.325	0.311	
9	20	7.80	300	300	2.66/O	0.324	0.311	$n_{in} \approx n_{140\,\mathrm{km}}$, Collisions
10	10	7.80	600	600	2.66/O	0.475	0.256	
11	10	7.80	150	600	2.66/O	0.474	0.256	
12	14.89	7.80	300	300	2.66/O	0.450	0.265	
13	4.44	7.80	300	300	2.66/O	0.825	0.088	
14	60.63	7.80	300	300	2.66/O	$\sim$0.05	$\sim$0.25	
15	34.48	7.80	300	300	2.66/O	0.141	0.323	
16	34.48	3.50	300	250	7.31/CO_2	0.100	0.306	
17	20	7.82	300	580.5	6.34/Ar	0.380	0.293	
18	20	7.82	300	580.5	0.665/He	0.063	0.281	
19	20	3.91	300	1451.25	$6.65/10 \times$ He	0.063	0.281	
20	20	7.82	300	580.5	4.65/N_2	0.307	0.315	
21	20	7.82	300	580.5	2.66/O	0.204	0.334	
22	20	7.82	300	580.5	5.31/O_2	0.333	0.308	

(If not mentioned, inter-particle collisions are switched off, assuming free molecular flow.)

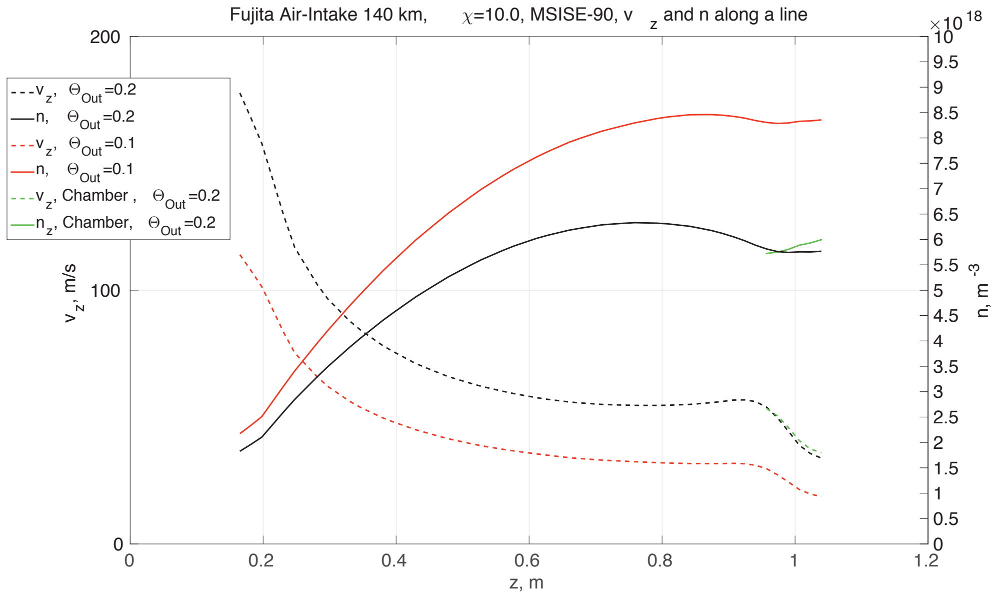

(a) Air-Intake, DSMC results at 140 km for JAXA Design, MSISE-90.

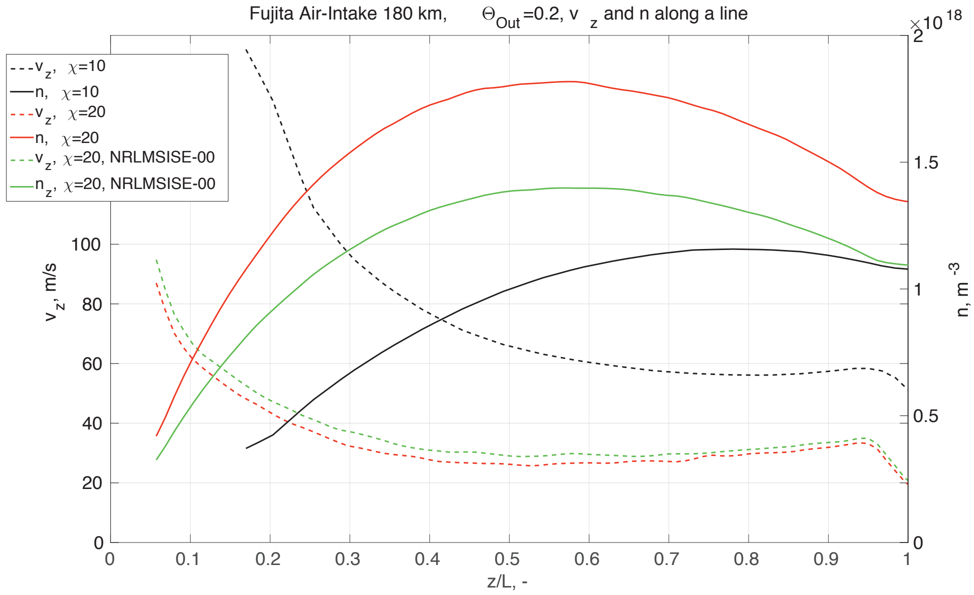

(b) Air-Intake, DSMC results at 180 km for JAXA Design, MSISE-90, NRLMSISE-00

Figure A1: Air-Intake, JAXA results, MSISE-90 and NRLMSISE-00.

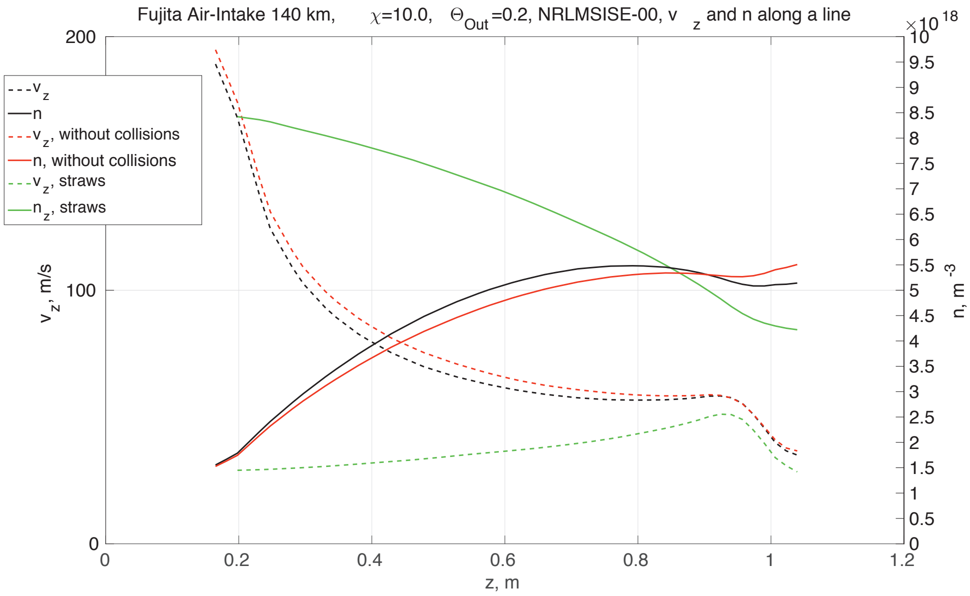

Figure A2: Air-Intake, DSMC results, JAXA Design with straws NRLMSISE-00.

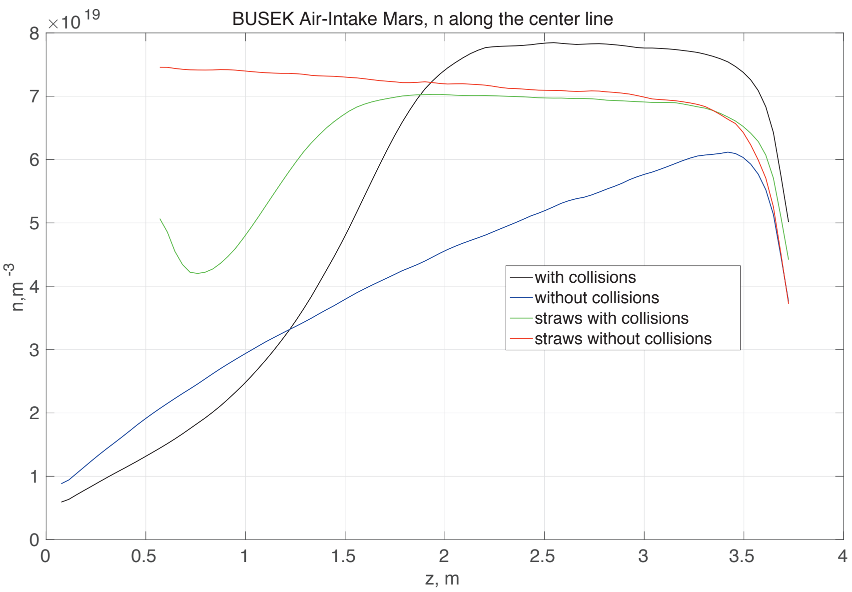

Figure A3: Density Along Center Line, BUSEK Design

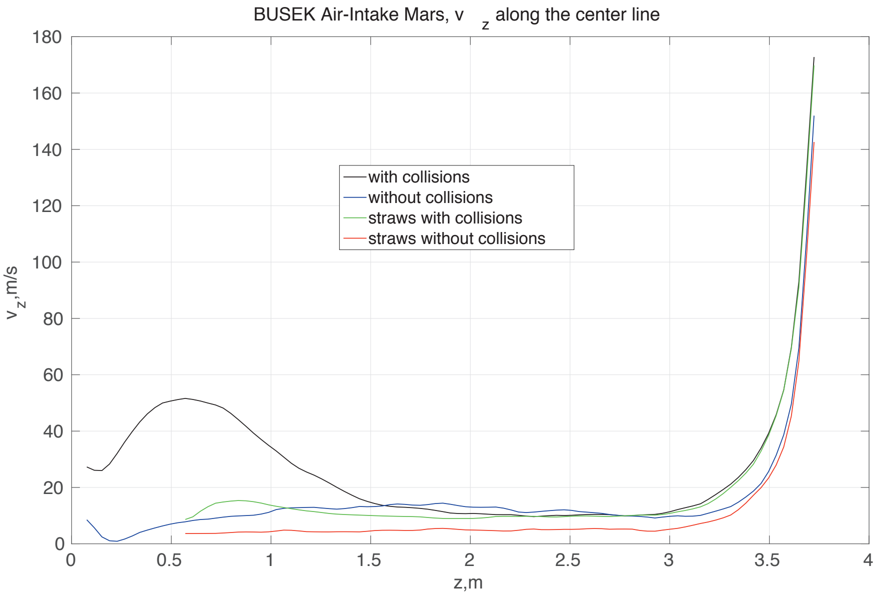

Figure A4: Velocity Along Center Line, BUSEK Design

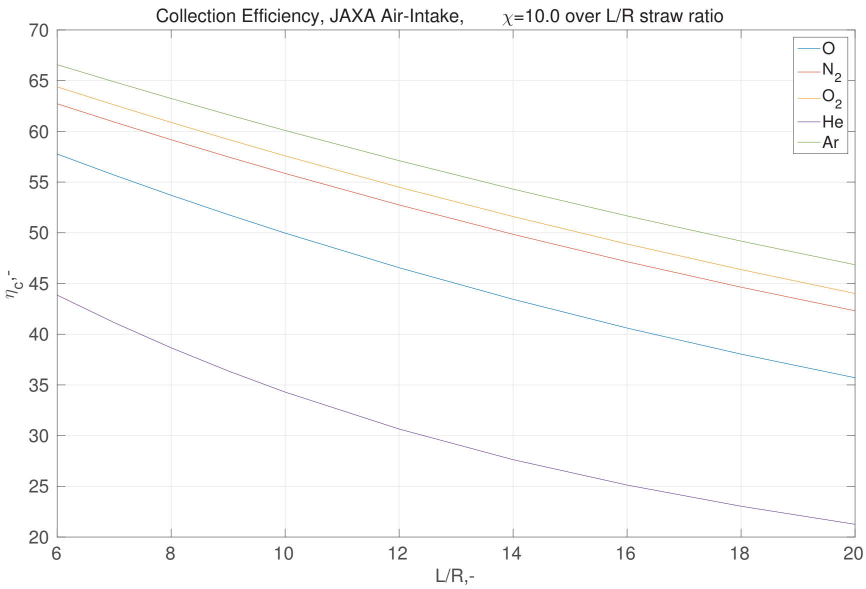

Figure A5: Balancing model applied to the JAXA Design, Collection Efficiency over L/R.

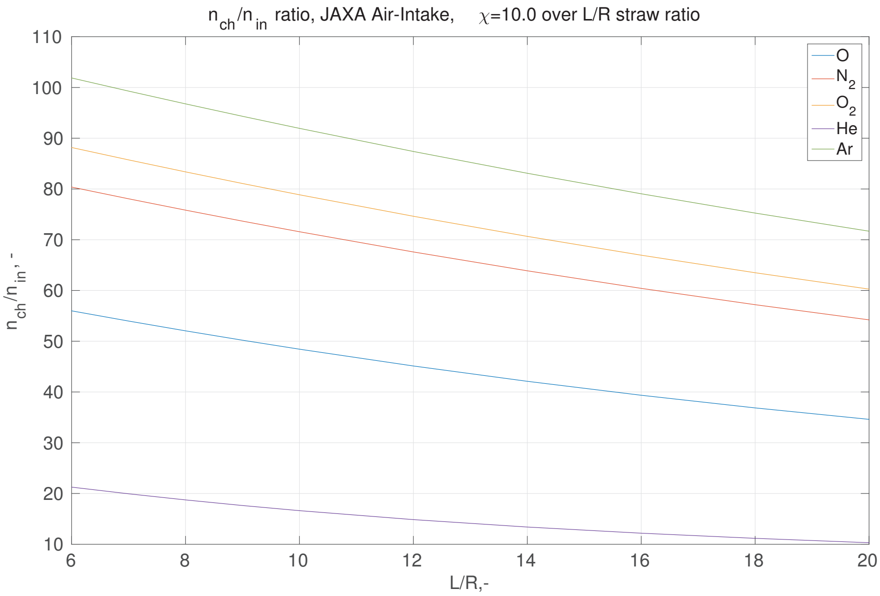

Figure A6: Balancing model applied to the JAXA Design, Number Density Ratio over L/R.

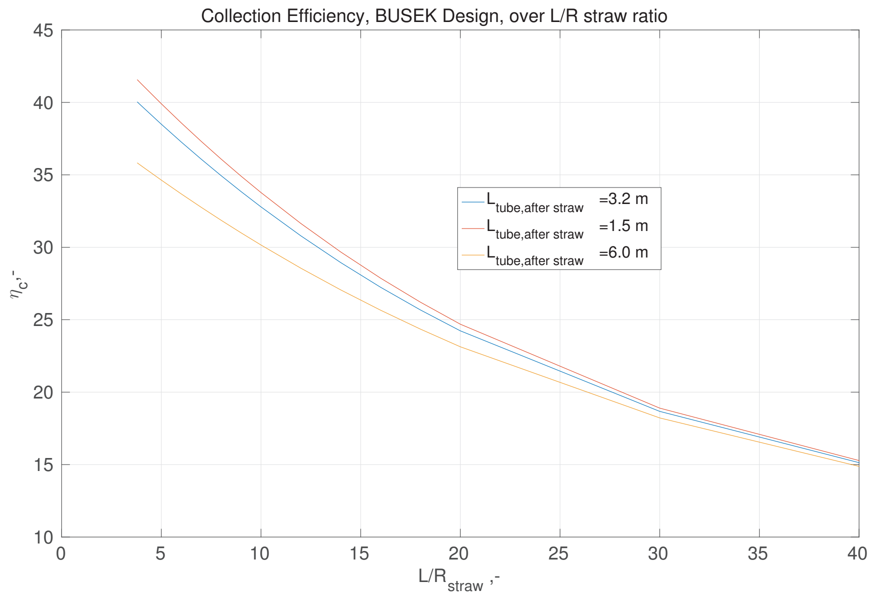

Figure A7: Balancing model applied to the BUSEK Design, Collection Efficiency over L/R.

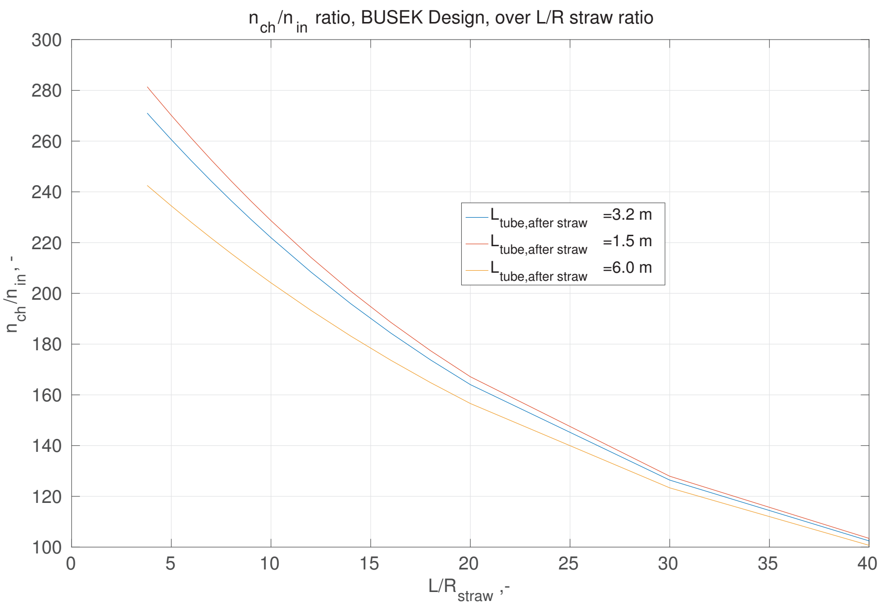

Figure A8: Balancing model applied to the BUSEK Design, Number Density Ratio over L/R.

Acknowledgments

F. Romano gratefully thanks the *Landesgraduiertenförderung* of the University of Stuttgart for the financial support; the authors acknowledge Mr. Yasuyoshi Hisamoto for the fruitful exchange of data regarding the japanese studies.

References

[1]G. A. Bird. *Molecular Gas Dynamics and the Direct Simulation of Gas Flows.* Clarendon, Oxford, 1994.

[2]P. Clausing. Über die strömung sehr verdünnter gase durch röhren von beliebiger länge. *Annalen der Physik*, 404(8):961–989, 1932.

[3]R. J. Cole. Complementary variational principles for Knudsen flow rates. *IMA Journal of Applied Mathematics*, pages 107–115, 1977.

[4]D Di Cara, A Santovincenzo, B Carnicero Dominguez, M Arcioni, A Caldwell, and I Roma. RAM electric propulsion for low earth orbit operation: an ESA study. 2007.

[5]Kazuhisa Fujita. Air-intake performance estimation of air-breathing ion engines. *Transactions of the Japan Society of Mechanical Engineers. B*, 70(700):3038–3044, dec 2004.

[6]Francisco Gonzalez-Galindo, Francois Forget, Monica Angelats I Coll, and Miguel Angel Lopez-Valverde. *The Martian Upper Atmosphere.* Stanford Linear Accelerator Center, Stanford, CA, USA, 2008.

[7]Yasuyoshi Hisamoto, Kazutaka Nishiyama, and Hitoshi Kuninaka. Design of air intake for air breathing ion engine. *63rd International Astronautical Congress, Naples, Italy.*, 2012.

[8]Kurt Hohman. Atmospheric breathing electric thruster for planetary exploration, 2012.

[9]Kurt Hohman. Atmospheric breathing electric thruster for planetary exploration. Presented as the NIAC Spring Symposium, 2012.

[10]Claus-Dieter Munz, Monika Auweter-Kurtz, Stefanos Fasoulas, Asim Mirza, Philip Ortwein, Marcel Pfeiffer, and Torsten Stindl. Coupled particle-in-cell and direct simulation monte carlo method for simulating reactive plasma flows. *Comptes Rendus Mcanique*, 342(1011):662 – 670, 2014. Theoretical and numerical approaches for Vlasov-maxwell equations.

[11]Dejan Petkow. *Modellierung von Teilchenkollisionen zur Berechnung hochverdünnter Plasmaströmungen.* PhD thesis, Universität Stuttgart, Holzgartenstr. 16, 70174 Stuttgart, 2011.

[12]J.M. Picone, A.E. Hedin, D.P. Drob, and A.C. Aikin. NRLMSISE-00 empirical model of the atmosphere: Statistical comparisons and scientific issues. *Journal of geophysical research*, 107(A12), 2002.

[13]Francesco Romano. System Analysis and Test-Bed for an Air-Breathing Electric Propulsion System. Master's thesis, Universität Stuttgart, University of Padova, 2014.

[14]T. Schönherr, K. Komurasaki, F. Romano, B. Massuti-Ballester, and G. Herdrich. Analysis of atmosphere-breathing electric propulsion. *Plasma Science, IEEE Transactions on*, 43(1):287–294, Jan 2015.